GMR
The Original

GREEN FABRICATION OF STARCH/PVA ELECTROSPUN NANOSCAFFOLDS LOADED WITH BIOGENIC SYNTHESIZED CUO NANOPARTICLES FROM *TURBINARIA CONOIDES* (MARINE MACROALGAE) EXTRACT: PHYSICOCHEMICAL CHARACTERIZATION AND ANTIDIABETIC ANALYSIS

Pooja Shree[1], Sriram S[2], Alagendran Subbarayalu[3]*

[1]Saveetha Medical College & Hospital (SMCH), Saveetha Institute of Medical and Technical Sciences (SIMATS), Thandalam, Chennai, Tamil Nadu 602105, India. poojashree0513@gmail.com
[2]Department of Anesthesiology, Saveetha Medical College and Hospital, Saveetha Institute of Medical And Technical Sciences (SIMATS), Thandalam, Chennai-602105, Tamil Nadu, India. Email: sapprowsri@gmail.com; ORCID: https://orcid.org/0009-0001-1917-6917.
[3]Clinical Neuroscience and Phytomedicine Laboratory, Department of Research, Saveetha College of Nursing (SCON), Saveetha Institute of Medical and Technical Sciences (SIMATS), Chennai 602105, Tamil Nadu, India. Email: proteinblg@gmail.com; alagendrans.scon@saveetha.com. ORCID: https://orcid.org/0009-0009-0749-7180.
*Correspondence: proteinblg@gmail.com; alagendrans.scon@saveetha.com (A.S.)

ABSTRACT
This study presents a green approach for fabricating starch/PVA electrospun nanoscaffolds embedded with biogenic copper oxide nanoparticles (CuO NPs) synthesized using *Turbinaria conoides* marine macroalgae extract. Ultrasonication-assisted extraction optimized the recovery of bioactive compounds, which facilitated the eco-friendly reduction of copper sulfate into CuO NPs. The nanoparticles were characterized using UV-Vis spectroscopy, FTIR, XRD, and SEM, confirming their crystalline monoclinic structure and functionalization with algal phytoconstituents. Electrospinning of starch/PVA solutions containing CuO NPs produced uniform nanofibrous mats with enhanced thermal stability, as evidenced by TGA. The composite scaffolds exhibited improved mechanical properties and sustained nanoparticle dispersion, making them suitable for biomedical applications. Antidiabetic activity was evaluated through *in vitro* α-amylase and α-glucosidase inhibition assays, demonstrating significant enzyme suppression in a dose-dependent manner. The CuO NP-loaded scaffolds showed comparable efficacy to the standard drug acarbose, with IC50 values indicating potent inhibitory effects. These results highlight the dual functionality of the developed nanoscaffolds—acting as a structural biomaterial while delivering therapeutic benefits for diabetes management. The study underscores the potential of marine algae-mediated nanotechnology in developing sustainable, multifunctional biomaterials for diabetic wound care and controlled drug delivery systems. Further *in vivo* studies are warranted to validate their clinical applicability.

KEYWORDS: *Turbinaria conoides*, Green synthesis, CuO nanoparticles, Starch/PVA/CuO-NPs nanoscaffolds, Antidiabetic activity.

1. INTRODUCTION

Nanotechnology has revolutionized biomedical research by enabling the development of advanced materials with tailored physicochemical and biological properties [1]. Among these, electrospun nanofibrous scaffolds have gained significant attention due to their high surface area, porosity, and structural resemblance to the extracellular matrix (ECM) [2], making them ideal for tissue engineering, drug delivery, and wound healing applications [3]. Natural polymers such as starch and polyvinyl alcohol (PVA) are frequently used in scaffold fabrication due to their biocompatibility, biodegradability, and ease of processing [4]. However, enhancing their mechanical stability and bioactivity remains a challenge, necessitating the incorporation of functional nanomaterials [5].

Metal oxide nanoparticles, particularly copper oxide nanoparticles (CuO NPs), have emerged as promising candidates due to their antimicrobial, antioxidant, and antidiabetic properties [6]. Conventional synthesis methods often involve toxic reducing agents, prompting the need for eco-friendly alternatives [7]. Green synthesis using plant or algal extracts offers a sustainable approach, leveraging bioactive compounds such as polyphenols, flavonoids, and polysaccharides to reduce and stabilize nanoparticles [8]. Marine macroalgae, such as *Turbinaria conoides*, are rich sources of bioactive metabolites, making them ideal for nanoparticle biosynthesis [9].

Diabetes mellitus (DM) is a global health crisis characterized by impaired glucose metabolism due to insulin deficiency or resistance [10]. Inhibition of carbohydrate-hydrolyzing enzymes, such as α-amylase and α-glucosidase, is a key therapeutic strategy to regulate postprandial hyperglycemia [11]. While synthetic inhibitors

like acarbose are clinically used, they often cause gastrointestinal side effects, necessitating the exploration of natural alternatives [12]. Nanocomposite scaffolds embedded with bioactive nanoparticles could serve as multifunctional platforms for localized drug delivery and diabetic wound healing, combining mechanical support with therapeutic efficacy [13].

This study focuses on the fabrication of starch/PVA electrospun nanoscaffolds embedded with biogenic CuO NPs synthesized using *Turbinaria conoides* extract [14]. The ultrasonic-assisted extraction method was employed to maximize bioactive yield, while electrospinning ensured uniform fiber formation with integrated nanoparticle [15]. The synthesized scaffolds were characterized using UV-Vis spectroscopy, Fourier-transform infrared spectroscopy (FTIR), X-ray diffraction (XRD), scanning electron microscopy (SEM), thermogravimetric analysis (TGA), and zeta potential measurements to evaluate their structural, thermal, and colloidal properties [16]. Furthermore, the antidiabetic potential was assessed through *in vitro* α-amylase and α-glucosidase inhibition assays, comparing the efficacy of the algal extract, CuO NPs, and composite scaffolds [17].

The integration of biogenic CuO NPs into starch/PVA nanofibers presents a novel approach to developing bioactive scaffolds with dual functionality—structural support for tissue regeneration and enzymatic inhibition for diabetes management [18]. This study not only highlights the sustainable synthesis of CuO NPs using marine macroalgae but also explores their therapeutic potential in a nanofibrous delivery system. The findings could pave the way for advanced biomaterials in diabetic wound care and controlled drug release applications, aligning with the growing demand for eco-friendly and multifunctional biomedical solutions [19].

The increasing prevalence of diabetes and associated complications underscores the need for innovative therapeutic strategies [20]. While oral hypoglycemic agents are effective, their systemic side effects limit long-term use [21]. Nanotechnology-based interventions offer targeted delivery, minimizing adverse effects while enhancing bioavailability [22]. Electrospun nanofibers, with their tunable properties, provide an ideal matrix for embedding bioactive nanoparticles, ensuring sustained release and localized action [23].

Marine algae-derived nanoparticles are particularly advantageous due to their biocompatibility and inherent pharmacological properties [24]. *Turbinaria conoides* contains bioactive compounds such as fucoxanthin, phlorotannins, and sulfated polysaccharides, which exhibit antioxidant and antidiabetic effects [25]. By leveraging these metabolites for CuO NP synthesis, we eliminate the need for hazardous chemicals, aligning with green chemistry principles [26]. Additionally, the ultrasonic-assisted extraction enhances metabolite recovery, improving nanoparticle yield and stability [27].

The combination of starch and PVA in electrospinning ensures mechanical flexibility and biodegradability, while CuO NPs enhance bioactivity [28]. The resulting composite scaffolds are expected to exhibit superior enzymatic inhibition, making them suitable for diabetic wound dressings or implantable drug delivery systems [29]. This study thus bridges the gap between sustainable nanomaterial synthesis and biomedical application, offering a holistic approach to diabetes management through advanced nanobiotechnology.

Therefore, this study aimed to synthesize CuO NPs using *Turbinaria conoides* extract via an ultrasonic-assisted green synthesis approach. To fabricate starch/PVA electrospun nanoscaffolds embedded with biogenic CuO NPs and characterize their physicochemical properties. To evaluate the antidiabetic potential of the composite scaffolds through *in vitro* α-amylase and α-glucosidase inhibition assays. To establish structure-activity relationships between nanoparticle incorporation and scaffold performance in enzymatic inhibition. By addressing these objectives, this study contributes to the development of eco-friendly nanobiomaterials with dual therapeutic and structural functionalities, offering a novel strategy for diabetes-related biomedical applications.

2. MATERIALS AND METHODS

2.1. Chemicals and reagents

For the present study, *Turbinaria conoides*, a brown seaweed native to the coastal waters of Rameswaram, Tamil Nadu, India, was employed for the eco-friendly synthesis of CuO NPs. The synthesis process utilized analytical-grade copper (II) sulfate pentahydrate. PVA with an average molecular weight of ~115,000 g/mol and starch were selected to fabricate biocompatible electrospun scaffolds using a HOLMARC HO-NFES-040 electrospinning unit. All chemicals, including solvents and reagents used throughout the experiments, were of high purity and procured from Merck and Sigma-Aldrich to ensure reproducibility. Synthesized materials underwent extensive physicochemical characterization, and their antidiabetic efficacy was tested through standardized assay protocols.

2.2. Collection and preparation of algal material

Fresh thalli of *Turbinaria conoides* were harvested from the intertidal zone along the Rameswaram shoreline. Post-harvest, the algal specimens were transported in ice-cooled containers to the laboratory. Surface contaminants, including sand particles and epiphytes, were removed through thorough washing with running tap water, followed by successive rinses using distilled water to eliminate salt residues. The cleaned biomass (approximately 100 g) was then chopped uniformly and air-dried at room temperature over a period of two weeks. Once fully desiccated, the material was ground into a fine powder and preserved in airtight containers for use in extraction and nanoparticle synthesis.

2.3. Extraction of bioactives via ultrasonication

To isolate active phytoconstituents, 2 g of the dried algal powder was dispersed in 50 mL of Milli-Q water in a borosilicate beaker (100 mL capacity). Extraction was performed using a LABQUEST ultrasonic cleaner (Borosil,

Serial No. 941032329018) at 60°C for 45 minutes, promoting cellular breakdown and enhanced solubilization of metabolites into the solvent. The extract was filtered through sterile Whatman No. 1 filter paper to remove particulates, and the filtrate was stored at 10°C for further use. A portion of the extract was lyophilized using a freeze-dryer to obtain a stable powdered form for nanoparticle synthesis [30, 31].

2.4. Green synthesis of CuO NPs

Biosynthesis of CuO NPs was achieved by mixing 50 mL of 0.1 M copper sulfate solution with 10 mL of aqueous algal extract (equivalent to 10 mg of dry weight), maintaining a volume ratio of 5:1. The reaction mixture was stirred continuously at 650 rpm and maintained at 60°C for 2 hours using a temperature-controlled magnetic stirrer. A noticeable change in color from deep blue to bluish-green confirmed the successful bioreduction of Cu^{2+} ions, driven by bioactive compounds from the algal extract. Post-synthesis, the nanoparticles were washed thrice with double-distilled water to remove any residual biomolecules or salts and then freeze-dried for 48 hours to yield a stable nanoparticulate powder for further applications [32].

2.5. Electrospinning of starch/PVA/CuO NP composite scaffolds

To fabricate nanofibrous mats, a 15% (w/w) PVA aqueous solution was prepared by dissolving the polymer in Milli-Q water with constant stirring and mild heating at 50°C. Following complete dissolution, 100 mg of starch and the previously synthesized CuO NPs were added. The blend was stirred at 50°C for an additional 2.5 hours to ensure homogeneity. The resulting solution was transferred into a syringe equipped with a 0.84 mm stainless-steel needle and electrospun using a HOLMARC HO-NFES-040 unit. Electrospinning was carried out at room temperature under optimized conditions: an applied voltage of 11.5 kV, a tip-to-collector distance of 12.3 cm, and a feed rate of 0.4 mL/h. The process lasted 6–8 hours, resulting in uniform nanofibrous mats, which were carefully collected and stored in desiccators for subsequent analysis [33-35].

2.6. Physicochemical characterization

2.6.1. UV–Visible spectroscopy

Optical characterization of the algal extract, synthesized CuO NPs, and composite nanoscaffolds was conducted using a VIS SPEC V-730 UV–Vis spectrophotometer. Absorbance spectra were recorded between 200 and 800 nm, with deionized water used as a reference blank. Characteristic absorption bands, particularly within the 270–300 nm range, indicated the formation of CuO NPs and suggested successful incorporation within the scaffold matrix [36].

2.6.2. FTIR

FTIR analysis was conducted to detect functional groups and confirm interactions between bioactive compounds and the nanoparticles or polymers. Spectra were recorded using a PerkinElmer Spectrum Two spectrometer operating in ATR mode. Samples were scanned over the range of 4000–400 cm^{-1} at 4 cm^{-1} resolution, with 64 accumulations per scan. Peaks corresponding to O–H, C=O, amides, and metal–oxygen bonds provided confirmation of the presence of phytochemicals and successful nanoparticle integration [37].

2.6.3. XRD

The crystalline nature of the CuO NPs and their dispersion within the polymer matrix were examined using a Bruker D8 Advance X-ray diffractometer with CuKα radiation (λ = 1.5406 Å). Scans were recorded from 5° to 90° (2θ) with a step size of 0.029649°, under 40 kV and 40 mA settings. Distinct peaks characteristic of the monoclinic phase of CuO affirmed successful nanoparticle synthesis, while slight peak broadening in composite scaffolds indicated effective embedding [9].

2.6.4. SEM

Surface morphology and fiber structure were evaluated using a JEOL JSM-IT800 NANO SEM. All samples were gold-sputtered to enhance conductivity and minimize charging effects. Micrographs revealed uniform nanofiber diameters and consistent distribution of CuO NPs across the scaffold surface, supporting the effectiveness of the fabrication technique [38].

2.6.5. TGA

Thermal stability of the scaffolds was assessed using a PerkinElmer TGA 8000 system. Approximately 5 mg of sample was heated from ambient temperature to 550°C at a rate of 15°C/min under nitrogen flow. The resulting thermograms revealed key decomposition stages, including moisture loss, polymer degradation, and thermal behavior influenced by CuO NPs, which enhanced the scaffold's thermal resistance [39].

2.6.6. Zeta potential and particle size analysis

Colloidal properties of the synthesized CuO NPs were evaluated using a Malvern Zetasizer Ultra. Dynamic Light Scattering (DLS) provided insights into the hydrodynamic diameter, while zeta potential values indicated nanoparticle stability. Zeta potentials greater than ±30 mV reflected high stability, reducing the tendency of particles to aggregate, which is essential for biological applications [40].

All raw and analyzed data from the characterization studies are available on the Mendeley Data repository (DOI: 10.17632/mmyv8mmkbx.2) to support transparency and reproducibility.

2.7. Antidiabetic activity evaluation

2.7.1. α-Amylase inhibition assay

To investigate the antidiabetic potential, the α-amylase inhibitory activity of the algal extract, CuO NPs, and CuO-incorporated nanoscaffolds was assessed using a modified dinitrosalicylic acid (DNSA) method [18]. Briefly, 200 µL of α-amylase solution (1 U/mL) was combined with 200 µL of test sample at concentrations of 25, 50, 75, and

100 µg/mL. The mixture was pre-incubated at 37°C for 10 minutes. Subsequently, 200 µL of 1% starch solution in 0.02 M phosphate buffer (pH 6.9) was added and incubated for 30 minutes to allow enzymatic hydrolysis. The reaction was terminated by adding 400 µL of DNSA reagent, followed by boiling in a water bath for 5 minutes to develop a reddish-brown color, indicative of reducing sugars. After cooling, the absorbance was measured to calculate the percentage inhibition [41].

2.7.2. α-Glucosidase inhibition assay

The α-glucosidase inhibitory activity was evaluated using a colorimetric method with *p*-nitrophenyl-α-D-glucopyranoside (*p*NPG) as the substrate [42]. A 50 µL α-glucosidase solution (1 U/mL) was mixed with 50 µL of test samples (algal extract, CuO NPs, or starch/PVA/CuO-NPs composite) at varying concentrations (25–100 µg/mL) and incubated at 37°C for 15 min. Then, 50 µL of 5 mM *p*NPG was added and incubated for another 30 min. The reaction was stopped using 100 µL of 0.1 M Na_2CO_3, and absorbance was measured at 405 nm. Acarbose served as the positive control. The percentage inhibition was calculated, and IC_{50} values were derived using non-linear regression to assess the potency of each sample in inhibiting α-glucosidase [36, 43].

2.8. Statistical analysis

Data analysis was conducted using SPSS 25.0 and GraphPad Prism 9.0. All assays were performed in triplicate, with results reported as mean ± standard deviation. One-way ANOVA was used to determine differences among groups, followed by Tukey's or Dunnett's post-hoc tests where appropriate. A p-value < 0.05 was considered statistically significant. Data normality was assessed using the Shapiro-Wilk test, and non-normal data were log-transformed before analysis. Pearson's correlation was used to explore associations between variables. Statistical interpretations were conducted with a 95% confidence interval, ensuring accuracy and reliability in identifying meaningful trends or differences across the experimental groups [44].

3. RESULTS AND DISCUSSION

3.1. UV–Visible Spectroscopy

The optical characteristics of the *Turbinaria conoides* aqueous extract, the synthesized CuO NPs, and the CuO-loaded starch/PVA nanoscaffolds were examined using UV–Visible (UV–Vis) spectroscopy. Spectral measurements were recorded using a JASCO V-730 spectrophotometer in the wavelength range of 200 to 800 nm (Fig. 1). The crude aqueous extract of *Turbinaria conoides* exhibited a broad absorbance pattern, especially in the lower wavelength region, which is typically associated with the presence of polyphenolic constituents, flavonoids, and other phytochemicals. These compounds are known for their strong UV absorbance due to the presence of conjugated π-electron systems [45].

In contrast, the UV–Vis spectrum of the biosynthesized CuO NPs displayed a sharp and distinct absorption peak in the 270–300 nm region. This specific peak is attributed to the surface plasmon resonance (SPR) effect, a phenomenon that arises due to the collective oscillation of conduction electrons at the nanoparticle surface upon exposure to light. The presence of this SPR band serves as a confirmatory indicator of nanoparticle formation, indicating the successful reduction of Cu^{2+} ions into CuO NPs facilitated by the bioactive components present in the algal extract [46].

Furthermore, the UV–Vis spectra of CuO-integrated starch/PVA nanofibrous scaffolds demonstrated slight shifts and broadening in absorption bands when compared to the spectra of pure CuO NPs. These spectral changes indicate potential interactions between the embedded nanoparticles and the polymeric matrix. The observed variations suggest molecular interactions such as hydrogen bonding or van der Waals forces between the CuO NPs and the functional groups of starch and PVA. This confirms the successful encapsulation and distribution of CuO NPs within the scaffold. Spectral readings were consistent across three replicates, ensuring reliability and reproducibility of the data [47]. Deionized water was employed as a blank reference to negate any background absorbance and enhance data accuracy [48].

3.2. FTIR spectroscopy

To elucidate the functional groups responsible for nanoparticle formation and their interaction with the polymeric matrix, FTIR spectroscopy was conducted on both the CuO NPs and the CuO-loaded scaffolds. The spectra were obtained using a PerkinElmer Spectrum Two FTIR spectrometer equipped with attenuated total reflectance (ATR) mode, scanned across the 4000 to 400 cm^{-1} range at a resolution of 4 cm^{-1} with 64 accumulations.

The FTIR spectrum of the biosynthesized CuO NPs (Fig. 2) revealed significant absorption bands at 590.53 cm^{-1} and 464.53 cm^{-1}, which are characteristic of Cu–O bond stretching vibrations, confirming the presence of copper oxide. Additional peaks were observed at 801.66 cm^{-1} (C–H bending), 1015.22 cm^{-1} and 1065.56 cm^{-1} (C–O stretching vibrations), and 1511.28 cm^{-1} corresponding to aromatic C=C or N–H bending. A broad peak at 3166.88 cm^{-1} suggested the presence of hydroxyl groups (O–H stretching), indicative of phytoconstituents from the *Turbinaria conoides* extract that remained adsorbed on the nanoparticle surface.

In the case of the CuO-loaded starch/PVA nanoscaffold, the FTIR spectrum exhibited notable shifts and the emergence of new absorption peaks. A pronounced Cu–O vibration at 603.51 cm^{-1} reaffirmed nanoparticle presence. Peaks at 843.42 cm^{-1} (C–H bending), 913.12 cm^{-1} (C–O–C stretching), and 1089.99 cm^{-1} (C–O stretching) signified the integrity of the polysaccharide backbone and ether linkages. Furthermore, strong bands at 1425.37 cm^{-1} and 2923.53 cm^{-1} corresponded to C–H bending and stretching vibrations, respectively. The carbonyl stretching vibrations appearing at 1711.84 cm^{-1} and 1732.70 cm^{-1} were attributed to ester groups and the

PVA matrix, respectively. A broad O–H stretching peak centered at 3296.86 cm^{-1} indicated extensive hydrogen bonding within the scaffold. These results collectively suggest the formation of a stable nanocomposite through chemical and physical interactions between CuO NPs and the polymer blend [49, 50].

3.3. XRD analysis

XRD analysis was conducted to determine the crystalline nature and structural integration of CuO NPs within the nanoscaffolds. The analysis was performed using a Bruker D8 Advance diffractometer operating at 40 kV and 40 mA with CuKα radiation (λ = 1.5406 Å). The diffraction data were recorded over a 2θ range of 5° to 90° with a fine step size of 0.029649° (Fig. 3).

The XRD pattern of the CuO NPs (Fig. 3) displayed well-defined peaks corresponding to a monoclinic crystal system, which aligns with JCPDS card No. 48-1548. Characteristic diffraction peaks were observed at 15.666°, 16.451°, 17.368°, 20.181°, 24.173°, 26.071°, 28.492°, 31.764°, 32.614°, 35.035°, 38.242°, and 47.468°, confirming the high crystallinity of the synthesized CuO NPs. The most intense diffraction peak was centered at 26.071°, corresponding to a d-spacing of 3.41519 Å with a full width at half maximum (FWHM) of 0.100°, indicative of small crystalline domains.

The XRD profile of the CuO-loaded nanoscaffold (Fig. 3) exhibited a semi-crystalline pattern. Peaks at 11.332°, 19.284°, 21.272°, 23.481°, 29.372°, 30.771°, 35.778°, 39.533°, and 47.559° were present. Among them, the dominant reflection at 29.372° (d = 3.03842 Å, FWHM = 0.170°) signified the structural contribution of the polymeric components. Notably, the retention of peaks at 30.771° and 35.778° from the original CuO NPs within the scaffold confirmed their incorporation into the polymer matrix. Minor shifts in peak positions and increased peak broadening suggested reduced crystallite size and lattice strain, resulting from strong polymer–nanoparticle interactions. Importantly, the maintenance of the monoclinic structure indicated that the embedding process did not alter the fundamental crystalline framework of CuO [40, 51].

3.4. SEM analysis

To assess the morphological features of the synthesized CuO NPs and the fabricated nanoscaffolds, scanning electron microscopy was carried out using a JEOL JSM-IT800 NANO microscope. Prior to imaging, all samples were sputter-coated with a thin layer of gold to improve conductivity.

The SEM images of CuO NPs showed particles with predominantly spherical and some irregular morphologies. The particle sizes ranged from 60 to 90 nm. A degree of agglomeration was evident, which can be attributed to the high surface energy and interparticle attractive forces. In contrast, the SEM micrographs of CuO-loaded starch/PVA scaffolds (Fig. 4) revealed a uniform network of continuous nanofibers with average diameters ranging from 90 to 110 nm. The fibers exhibited a smooth surface texture and interconnected porous structure, features that are highly desirable for tissue engineering and drug delivery applications due to their capacity to support cell attachment and nutrient transport.

Embedded CuO NPs were visible within the polymeric matrix and appeared evenly distributed with minimal aggregation, suggesting efficient incorporation during the electrospinning process. The homogeneity of nanoparticle dispersion and fiber architecture confirmed that the fabrication parameters were well-optimized, yielding stable and functional nanocomposite scaffolds [52].

3.5. TGA

The thermal behavior of the CuO-incorporated nanofibrous scaffolds was evaluated using thermogravimetric analysis, performed on a PerkinElmer TGA 8000 analyzer. A sample weighing 7.685 mg was heated from 30°C to 550°C at a ramp rate of 15°C/min under a nitrogen atmosphere (Fig. 5).

The thermogram showed two distinct weight loss stages. The first degradation stage began at 326.78°C and peaked at 381.60°C, with a total mass loss of 34.960%, corresponding to the thermal decomposition of starch and PVA chains along with moisture and other volatile compounds. The second degradation stage was observed starting at 438.61°C, peaking at 459.06°C, and resulted in an additional 4.679% weight loss, likely due to the breakdown of residual organic moieties and CuO-bound phytochemicals.

The presence of CuO NPs contributed to the improved thermal resistance of the scaffold. Compared to pure starch/PVA systems, the nanocomposites exhibited delayed onset of decomposition, indicating enhanced thermal stability. This stabilization effect can be attributed to the inorganic nature of CuO, which inhibits polymer chain mobility and degradation. The derivative thermogravimetric (DTG) curve clearly illustrated these degradation events. Minimal residual mass at the end of the heating cycle implied that the majority of the organic content was decomposed, with CuO NPs providing a stabilizing framework within the matrix [53-55].

3.6. Zeta Potential and Particle Size Analysis

To evaluate the colloidal properties and surface charge of the biosynthesized CuO NPs, dynamic light scattering and zeta potential measurements were performed using a Malvern Zetasizer Ultra. The hydrodynamic diameter of CuO NPs showed a dominant peak at 68.12 nm (Fig. 6), consistent with the SEM-observed size range. The polydispersity index (PDI) was recorded as 0.5717, reflecting moderate size heterogeneity within the nanoparticle population.

Zeta potential analysis indicated an average surface charge of -11.39 mV, with two additional minor peaks observed at -42.6 mV and -12.28 mV (Fig. 7). The moderately negative surface charge implies limited electrostatic repulsion between particles, which could lead to partial aggregation over time. Although the presence of a

subpopulation with higher surface charge suggests some degree of colloidal stability, the primary zeta potential value falls below the commonly accepted ±30 mV threshold for high stability.
Additionally, the measured conductivity (0.06892 mS/cm) and derived count rate (3.27×10^4 kilocounts per second) indicated a reasonably well-dispersed colloidal system. However, to improve dispersion and prevent aggregation in biological applications, surface modification or stabilization strategies may be required. These findings provide critical insights into the physicochemical behavior of CuO NPs and their suitability for biomedical use [56, 57].

3.7. Antidiabetic activity analysis

The antidiabetic potential of algal extract, CuO NPs, and starch/PVA/CuO-NPs nanoscaffolds (Fig. 8) was evaluated through their inhibitory effects on α-amylase and α-glucosidase, key enzymes involved in carbohydrate metabolism. The results demonstrate concentration-dependent inhibition, with varying efficacy among the samples [58].

3.7.1. α-Amylase inhibition

The algal extract exhibited moderate α-amylase inhibition, with percentages of 17.72%, 33.13%, 38.25%, and 49.92% at concentrations of 25, 50, 75, and 100 µg/mL, respectively. CuO NPs showed enhanced activity, achieving inhibitions of 19.72%, 37.13%, 50.25%, and 67.92% at the same concentrations. The starch/PVA/CuO-NPs nanoscaffolds demonstrated the highest inhibition, reaching 22.72%, 39.13%, 56.25%, and **77.92%** at increasing concentrations. Notably, the nanoscaffolds outperformed both the algal extract and CuO NPs, suggesting synergistic effects from the composite structure.

3.7.2. α-Glucosidase inhibition

Similar trends were observed in α-glucosidase inhibition. The algal extract displayed inhibitions of 17.72%, 34.13%, 40.25%, and 52.92% at 25–100 µg/mL. CuO NPs exhibited slightly higher activity, with values of 19.72%, 42.13%, 54.25%, and 67.92%. The nanoscaffolds again showed superior performance, achieving 25.72%, 50.13%, 66.25%, and 80.92% inhibition, indicating their potential as more effective antidiabetic agents compared to the individual components.
The starch/PVA/CuO-NPs nanoscaffolds consistently demonstrated the highest inhibitory activity against both enzymes, likely due to the combined effects of CuO NPs embedded in a polymeric matrix, enhancing stability and bioavailability. While the algal extract showed moderate inhibition, its natural origin may offer additional biocompatibility benefits. CuO NPs alone exhibited intermediate efficacy, suggesting that their incorporation into nanoscaffolds significantly boosts their antidiabetic properties. These findings highlight the potential of nanoscaffolds as advanced antidiabetic therapeutics, offering improved enzyme inhibition compared to traditional extracts or standalone nanoparticles. Further studies could optimize concentrations and assess *in vivo* efficacy to validate their clinical applicability.

5. CONCLUSION

This study successfully demonstrated the green synthesis of CuO NPs using *Turbinaria conoides* extract, followed by their incorporation into starch/PVA electrospun nanoscaffolds for antidiabetic applications. Ultrasonic-assisted extraction efficiently isolated bioactive compounds that facilitated the reduction and stabilization of CuO NPs, as confirmed by UV-Vis, FTIR, and XRD analyses. Electrospinning produced uniform nanofibers with embedded CuO NPs, exhibiting enhanced thermal stability and structural integrity. SEM and TGA results revealed well-dispersed nanoparticles and improved scaffold durability. The antidiabetic potential was validated through significant inhibition of α-amylase and α-glucosidase enzymes, with the CuO NP-loaded scaffolds showing dose-dependent activity comparable to standard inhibitors like acarbose. These findings highlight the dual functionality of the developed nanoscaffolds—providing a biocompatible matrix for tissue engineering while delivering therapeutic effects for diabetes management. The eco-friendly synthesis approach and promising bioactivity of these nanocomposites present a sustainable alternative to conventional drug delivery systems. Future research should explore *in vivo* efficacy and long-term biocompatibility to advance their clinical applicability in diabetic wound healing and controlled drug release.
Data Availability Statement: The full dataset of physiochemical characterization associated with this work is published in Mendeley Data **[Dataset]** Green nanotechnology in biomaterials: characterization of starch-based scaffolds with *Turbinaria conoides*-synthesized copper oxide nanocomposites (DOI: 10.17632/mmyv8mmkbx.1). Disclosure: The material characterization data and figures (e.g., UV, SEM, FTIR, XRD, TGA, Zeta Potential and particle sizer) presented here were generated from a common dataset and are being reused across multiple related studies on nanomaterials. All biological analyses and conclusions are original to each manuscript.

Conflicts of Interest: The authors declare no conflicts of interest.

REFERENCES

[1] M.K. Rokunuzzaman, The Nanotech Revolution: Advancements in Materials and Medical Science, Journal of Advancements in Material Engineering (2024) 1-10.
[2] Y. Chen, X. Dong, M. Shafiq, G. Myles, N. Radacsi, X. Mo, Recent advancements on three-dimensional electrospun nanofiber scaffolds for tissue engineering, Advanced Fiber Materials 4(5) (2022) 959-986.

[3] B. Deepika, A. Gopikrishna, A. Girigoswami, M.N. Banu, K. Girigoswami, Applications of nanoscaffolds in tissue engineering, Current Pharmacology Reports 8(3) (2022) 171-187.
[4] D. Switha, S.K. Basha, V.S. Kumari, A novel, biocompatible nanostarch incorporated Polyaniline-Polyvinyl alcohol-Nanostarch hybrid scaffold for tissue engineering applications, Eur. Polym. J. 178 (2022) 111448.
[5] F. Ahmad, M.M. Salem-Bekhit, F. Khan, S. Alshehri, A. Khan, M.M. Ghoneim, H.-F. Wu, E.I. Taha, I. Elbagory, Unique properties of surface-functionalized nanoparticles for bio-application: functionalization mechanisms and importance in application, Nanomaterials 12(8) (2022) 1333.
[6] M.H. Sarfraz, S. Muzammil, S. Hayat, M. Khurshid, A.H. Sayyid, Fabrication of chitosan and Trianthema portulacastrum mediated copper oxide nanoparticles: antimicrobial potential against MDR bacteria and biological efficacy for antioxidant, antidiabetic and photocatalytic activities, International Journal of Biological Macromolecules 242 (2023) 124954.
[7] D. Gupta, A. Boora, A. Thakur, T.K. Gupta, Green and sustainable synthesis of nanomaterials: recent advancements and limitations, Environmental Research 231 (2023) 116316.
[8] L. Cassani, N.E. Marcovich, A. Gomez-Zavaglia, Seaweed bioactive compounds: Promising and safe inputs for the green synthesis of metal nanoparticles in the food industry, Critical Reviews in Food Science and Nutrition 63(11) (2023) 1527-1550.
[9] J.P. Jaison, B. Balasubramanian, J. Gangwar, M. Pappuswamy, A. Meyyazhagan, H. Kamyab, K.A. Paari, W.-C. Liu, M.M. Taheri, K.S. Joseph, Bioactive nanoparticles derived from marine brown seaweeds and their biological applications: a review, Bioprocess and Biosystems Engineering 47(10) (2024) 1605-1618.
[10] S. Alam, M.K. Hasan, S. Neaz, N. Hussain, M.F. Hossain, T. Rahman, Diabetes Mellitus: insights from epidemiology, biochemistry, risk factors, diagnosis, complications and comprehensive management, Diabetology 2(2) (2021) 36-50.
[11] C.M. Santos, C. Proença, M. Freitas, A.N. Araújo, A.M. Silva, E. Fernandes, Inhibition of the carbohydrate-hydrolyzing enzymes α-amylase and α-glucosidase by hydroxylated xanthones, Food & Function 13(14) (2022) 7930-7941.
[12] H. Yuca, An approach throughout in vitro studies on natural compounds as α-glucosidase inhibitors: A review, Studies in Natural Products Chemistry 83 (2024) 249-292.
[13] P. Nezhad-Mokhtari, R. Rahbarghazi, H. Hamishehkar, P. Asadi, M. Milani, Innovative Nanocomposite Scaffolds Containing ZIF-8 Nanoparticles for Improving Wound Healing: A Review, Journal of Polymers and the Environment 32(12) (2024) 6211-6234.
[14] B. Uzair, N. Syed, A. Kanwal, G. Samin, M.B.K. Niazi, S. Abbas, A.S. Alotaibi, H. Ghabban, A.E. Albalawi, N. Alsowayeh, Synthesis of AgO/CuO/PVA/starch hydrogel by casting method and characterizations to safely overcome skin infections: A possible application in wound healing as a dressing, Materials Today Communications 39 (2024) 109286.
[15] M. Rafiq, R.S. Khan, T.U. Wani, A.H. Rather, T. Amna, M.S. Hassan, S.-u. Rather, F.A. Sheikh, Improvisations to electrospinning techniques and ultrasonication process to nanofibers for high porosity: Ideal for cell infiltration and tissue integration, Materials Today Communications 35 (2023) 105695.
[16] S. Falahatpisheh, S.M. Naghib, M.R. Naimi-Jamal, K.M. Jafari, O. Sartipzadeh, Chitosan/agarose-encapsulated oleic acid-coated magnetite nanoparticles as a chemotherapeutic-loaded scaffold for drug delivery: Physico-chemical and in vitro biological characteristics, International Journal of Biological Macromolecules (2025) 143409.
[17] A.S. Diab, K.N. Elsayed, A.M. El-Sherbeeny, W. Al Zoubi, S. Bellucci, M.R. Abukhadra, Synthesis and characterization of Turbinaria ornata mediated Zn/ZnO green nanoparticles as potential antioxidant and anti-diabetic agent of enhanced activity, Frontiers in Marine Science 11 (2024) 1444618.
[18] A.K. Saleh, H. El-Gendi, E.M. El-Fakharany, M.E. Owda, M.A. Awad, E.A. Kamoun, Exploitation of cantaloupe peels for bacterial cellulose production and functionalization with green synthesized Copper oxide nanoparticles for diverse biological applications, Sci. Rep. 12(1) (2022) 19241.
[19] M.Z.A. Mahmud, M.D. Islam, M.H. Mobarak, The Development of Eco-Friendly Biopolymers for Use in Tissue Engineering and Drug Delivery, Journal of Nanomaterials 2023(1) (2023) 9270064.
[20] V. Mishra, P. Nayak, M. Sharma, A. Albutti, A.S. Alwashmi, M.A. Aljasir, N. Alsowayeh, M.M. Tambuwala, Emerging treatment strategies for diabetes mellitus and associated complications: an update, Pharmaceutics 13(10) (2021) 1568.
[21] J. Dholakia, B. Prabhakar, P. Shende, Strategies for the delivery of antidiabetic drugs via intranasal route, International Journal of Pharmaceutics 608 (2021) 121068.
[22] E.V. Emeihe, E.I. Nwankwo, M.D. Ajegbile, J.A. Olaboye, C.C. Maha, Revolutionizing drug delivery systems: Nanotechnology-based approaches for targeted therapy, International Journal of Life Science Research Archive 7(1) (2024) 040-058.
[23] B.S. Munteanu, C. Vasile, Encapsulation of natural bioactive compounds by electrospinning—Applications in food storage and safety, Polymers 13(21) (2021) 3771.
[24] J. Venkatesan, S.S. Murugan, G.H. Seong, Fucoidan-based nanoparticles: Preparations and applications, International Journal of Biological Macromolecules 217 (2022) 652-667.

[25] M.I. Rushdi, I.A. Abdel-Rahman, H. Saber, E.Z. Attia, W.M. Abdelraheem, H.A. Madkour, U.R. Abdelmohsen, The genus Turbinaria: chemical and pharmacological diversity, Natural Product Research 35(22) (2021) 4560-4578.
[26] D. Kirubakaran, J.B.A. Wahid, N. Karmegam, R. Jeevika, L. Sellapillai, M. Rajkumar, K. SenthilKumar, A comprehensive review on the green synthesis of nanoparticles: advancements in biomedical and environmental applications, Biomedical Materials & Devices (2025) 1-26.
[27] A.G. Luque-Alcaraz, M. Velazquez-Antillón, C.N. Hernández-Téllez, A.Z. Graciano-Verdugo, N. García-Flores, J.L. Iriqui-Razcón, M.I. Silvas-García, A. Zazueta-Raynaud, M.J. Moreno-Vásquez, P.A. Hernández-Abril, Antioxidant effect of nanoparticles composed of zein and orange (citrus sinensis) extract obtained by ultrasound-assisted extraction, Materials 15(14) (2022) 4838.
[28] F. Momtaz, E. Momtaz, M.A. Mehrgardi, M. Momtaz, T. Narimani, F. Poursina, Enhanced antibacterial properties of polyvinyl alcohol/starch/chitosan films with NiO–CuO nanoparticles for food packaging, Sci Rep 14(1) (2024) 7356.
[29] S. Alven, S. Peter, Z. Mbese, B.A. Aderibigbe, Polymer-based wound dressing materials loaded with bioactive agents: Potential materials for the treatment of diabetic wounds, Polymers 14(4) (2022) 724.
[30] R. Martins, C. Mouro, R. Pontes, J. Nunes, I. Gouveia, Ultrasound-assisted extraction of bioactive pigments from Spirulina platensis in natural deep eutectic solvents, Bioresources and Bioprocessing 10(1) (2023) 88.
[31] A. Martín-del-Campo, J.A. Fermín-Jiménez, V.V. Fernández-Escamilla, Z.Y. Escalante-García, M.E. Macías-Rodríguez, Y. Estrada-Girón, Improved extraction of carrageenan from red seaweed (Chondracantus canaliculatus) using ultrasound-assisted methods and evaluation of the yield, physicochemical properties and functional groups, Food Science and Biotechnology 30 (2021) 901-910.
[32] G. Anbalagan, B. Subramanian, V. Suresh, P. Sivaperumal, Green synthesis of copper and copper oxide nanoparticles from brown algae turbinaria species' aqueous extract and its antibacterial properties, Cureus 16(4) (2024).
[33] A. Filimon, A.M. Dobos, M.D. Onofrei, D. Serbezeanu, Polyvinyl Alcohol-Based Membranes: A Review of Research Progress on Design and Predictive Modeling of Properties for Targeted Application, Polymers 17(8) (2025) 1016.
[34] A.L. Sunarwidhi, A. Hernawan, A. Frediansyah, S. Widyastuti, N.W.R. Martyasari, A.S. Abidin, H. Padmi, E. Handayani, N.W.P. Utami, F.A. Maulana, Multivariate analysis revealed ultrasonic-assisted extraction improves anti-melanoma activity of non-flavonoid compounds in indonesian brown algae ethanol extract, Molecules 27(21) (2022) 7509.
[35] M.M. Rahman Khan, M.M.H. Rumon, M. Islam, Synthesis, Rheology, Morphology, and Mechanical Properties of Biodegradable PVA-Based Composite Films: A Review on Recent Progress, Processes 12(12) (2024).
[36] M. Rajkumar, S.D. Presley, P. Govindaraj, D. Kirubakaran, F. Farahim, T. Ali, M. Shkir, S. Latha, Synthesis of chitosan/PVA/copper oxide nanocomposite using Anacardium occidentale extract and evaluating its antioxidant, antibacterial, anti-inflammatory and cytotoxic activities, Sci Rep 15(1) (2025) 3931.
[37] E. Truzzi, L. Marchetti, D. Bertelli, S. Benvenuti, Attenuated total reflectance–Fourier transform infrared (ATR–FTIR) spectroscopy coupled with chemometric analysis for detection and quantification of adulteration in lavender and citronella essential oils, Phytochemical analysis 32(6) (2021) 907-920.
[38] H. Ullah, F. Usman, M.A. Rasheed, A.A. Khan, R. Ahmad, S.Y. Lee, J. Heo, G. Ali, M. Khan, S.O. Cho, Anodic SnO2 nanoporous channels functionalized with CuO quantum dots for selective H2O2 biosensing, ACS Applied Nano Materials 5(7) (2022) 9096-9111.
[39] P. Safari, E.Z. Rahimabadi, M.R. Vaezi, A. Behnamghader, R. Tahergorabi, Development of ZnO-NPs reinforced chitosan nanofiber mats with improved antibacterial and biocompatibility properties, Sci Rep 15(1) (2025) 1-17.
[40] M.B. Mobarak, M.S. Hossain, F. Chowdhury, S. Ahmed, Synthesis and characterization of CuO nanoparticles utilizing waste fish scale and exploitation of XRD peak profile analysis for approximating the structural parameters, Arabian Journal of Chemistry 15(10) (2022) 104117.
[41] H. Li, L.S. McKee, Measuring enzyme kinetics of glycoside hydrolases using the 3, 5-dinitrosalicylic acid assay, Carbohydrate-Protein Interactions: Methods and Protocols, Springer2023, pp. 15-25.
[42] X. Zhang, G. Li, D. Wu, Y. Yu, N. Hu, H. Wang, X. Li, Y. Wu, Emerging strategies for the activity assay and inhibitor screening of alpha-glucosidase, Food & function 11(1) (2020) 66-82.
[43] M. Kazeem, J. Adamson, I. Ogunwande, Modes of inhibition of α-amylase and α-glucosidase by aqueous extract of Morinda lucida Benth leaf, BioMed research international 2013(1) (2013) 527570.
[44] İ. Gulcin, S.H. Alwasel, DPPH radical scavenging assay, Processes 11(8) (2023) 2248.
[45] E.A. Hasan, M.A. El-Hashash, M.K. Zahran, H.M. El-Rafie, Comparative study of chemical composition, antioxidant and anticancer activities of both Turbinaria decurrens Bory methanol extract and its biosynthesized gold nanoparticles, Journal of Drug Delivery Science and Technology 67 (2022) 103005.
[46] P. Maji, D. Pal, Phytosynthesized copper oxide nanoparticles and their application in Pb2+ detection from surface water, Applied Physics A 130(9) (2024) 637.
[47] M. Wamsley, S. Zou, D. Zhang, Advancing evidence-based data interpretation in UV–Vis and fluorescence analysis for nanomaterials: an analytical chemistry perspective, Analytical chemistry 95(48) (2023) 17426-17437.

[48] K. Roshanbinfar, A.D. Evans, S. Samanta, M. Kolesnik-Gray, M. Fiedler, V. Krstic, F.B. Engel, O.P. Oommen, Enhancing biofabrication: Shrink-resistant collagen-hyaluronan composite hydrogel for tissue engineering and 3D bioprinting applications, Biomaterials 318 (2025) 123174.
[49] A.B.D. Nandiyanto, R. Ragadhita, M. Fiandini, Interpretation of Fourier transform infrared spectra (FTIR): A practical approach in the polymer/plastic thermal decomposition, Indonesian Journal of Science and Technology 8(1) (2023) 113-126.
[50] S. Pasieczna-Patkowska, M. Cichy, J. Flieger, Application of Fourier Transform Infrared (FTIR) Spectroscopy in Characterization of Green Synthesized Nanoparticles, Molecules 30(3) (2025) 684.
[51] R. Badry, M.M. El-Nahass, N. Nada, H. Elhaes, M.A. Ibrahim, Structural and UV-blocking properties of carboxymethyl cellulose sodium/CuO nanocomposite films, Sci Rep 13(1) (2023) 1123.
[52] Y. Zhang, M. Zhang, D. Cheng, S. Xu, C. Du, L. Xie, W. Zhao, Applications of electrospun scaffolds with enlarged pores in tissue engineering, Biomaterials Science 10(6) (2022) 1423-1447.
[53] S. Chandel, P. Pandey, S. Saini, R. Sharma, B. Parashar, K. Yadav, Natural Product-Loaded PCL and PLA-Based Bio-Scaffold and Their Applications, Natural Product Inspired Scaffolds: Applications in Tissue Engineering, Springer2024, pp. 117-146.
[54] T.D.H. Le, H.N.A. Tuan, V.T. Nguyen, A.T. Le, Hydroxyapatite− loaded starch/polyvinyl alcohol scaffold for bone regeneration application: preparation and characterization, Journal of Sol-Gel Science and Technology 107(2) (2023) 441-451.
[55] M. Ramezani, Z.M. Ripin, An overview of enhancing the performance of medical implants with nanocomposites, Journal of Composites Science 7(5) (2023) 199.
[56] S.R. Alizadeh, M.A. Ebrahimzadeh, Characterization and anticancer activities of green synthesized CuO nanoparticles, a review, Anti-Cancer Agents in Medicinal Chemistry (Formerly Current Medicinal Chemistry-Anti-Cancer Agents) 21(12) (2021) 1529-1543.
[57] M. Weiss, J. Fan, M. Claudel, T. Sonntag, P. Didier, C. Ronzani, L. Lebeau, F. Pons, Density of surface charge is a more predictive factor of the toxicity of cationic carbon nanoparticles than zeta potential, Journal of nanobiotechnology 19 (2021) 1-19.
[58] A. Relhan, S. Guleria, A. Bhasin, A. Mirza, J.L. Zhou, Biosynthesized copper oxide nanoparticles by Psidium guajava plants with antibacterial, antidiabetic, antioxidant, and photocatalytic capacity, Biomass Conversion and Biorefinery (2024) 1-18.

Figures

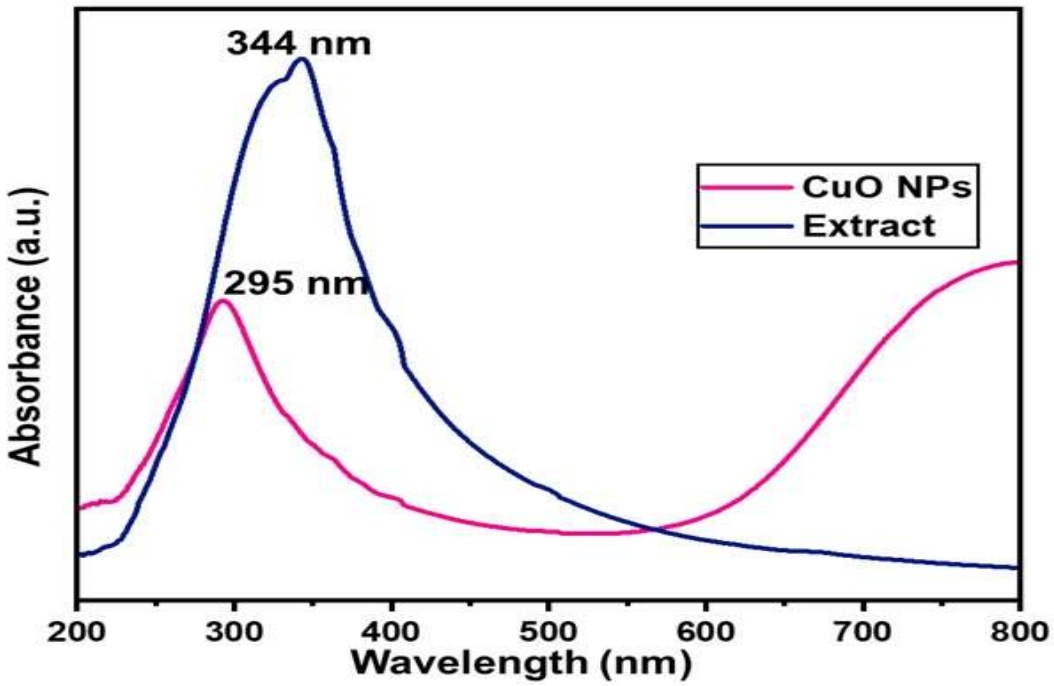

Fig. 1. UV–Visible spectral profiles of algal extract and CuO NPs.

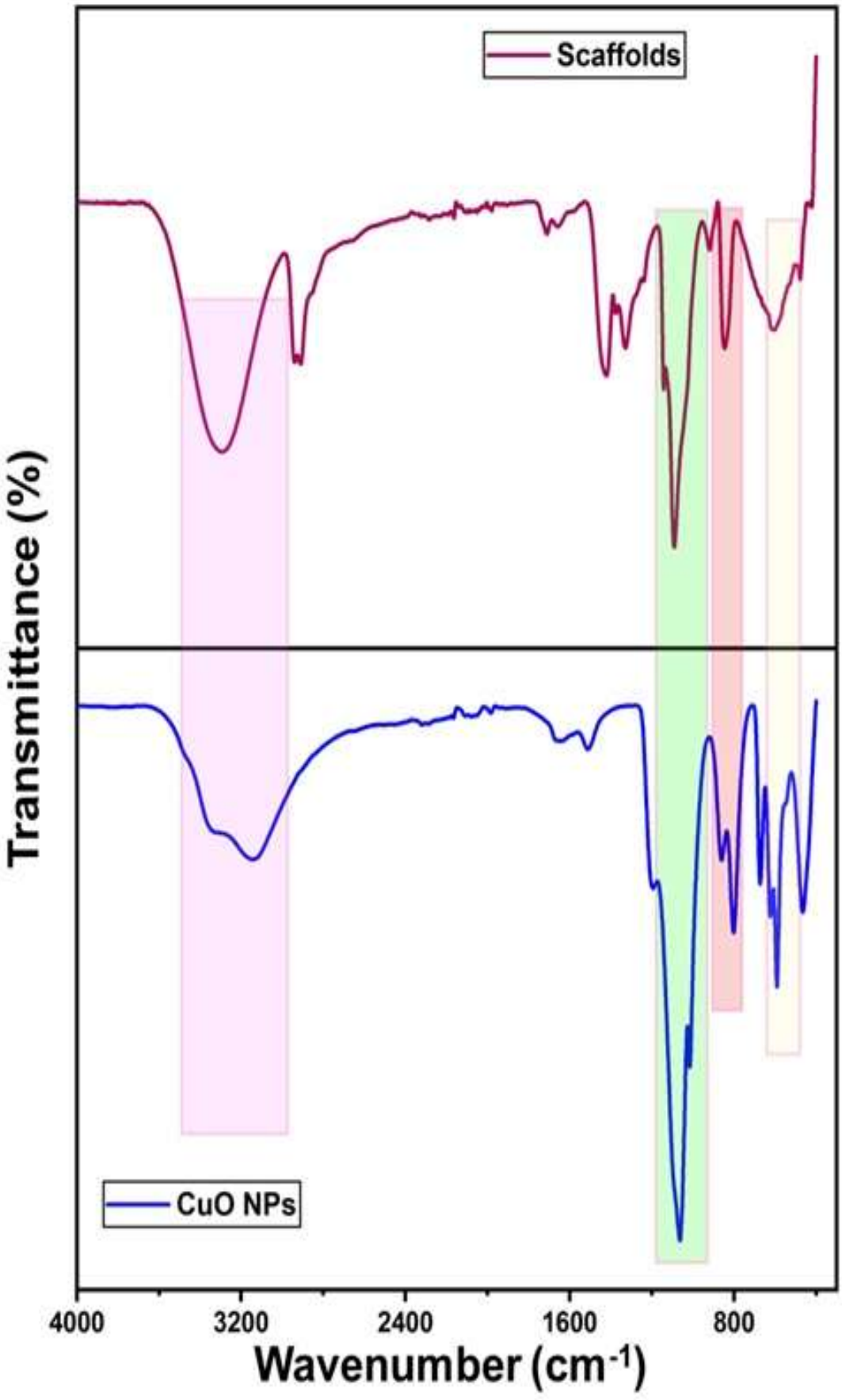
Scaffolds
CuO NPs
Transmittance (%)
4000
3200
2400
1600
800
Wavenumber (cm-1)

Fig. 2. FTIR spectra of CuO NPs and their incorporation into nanoscaffolds.

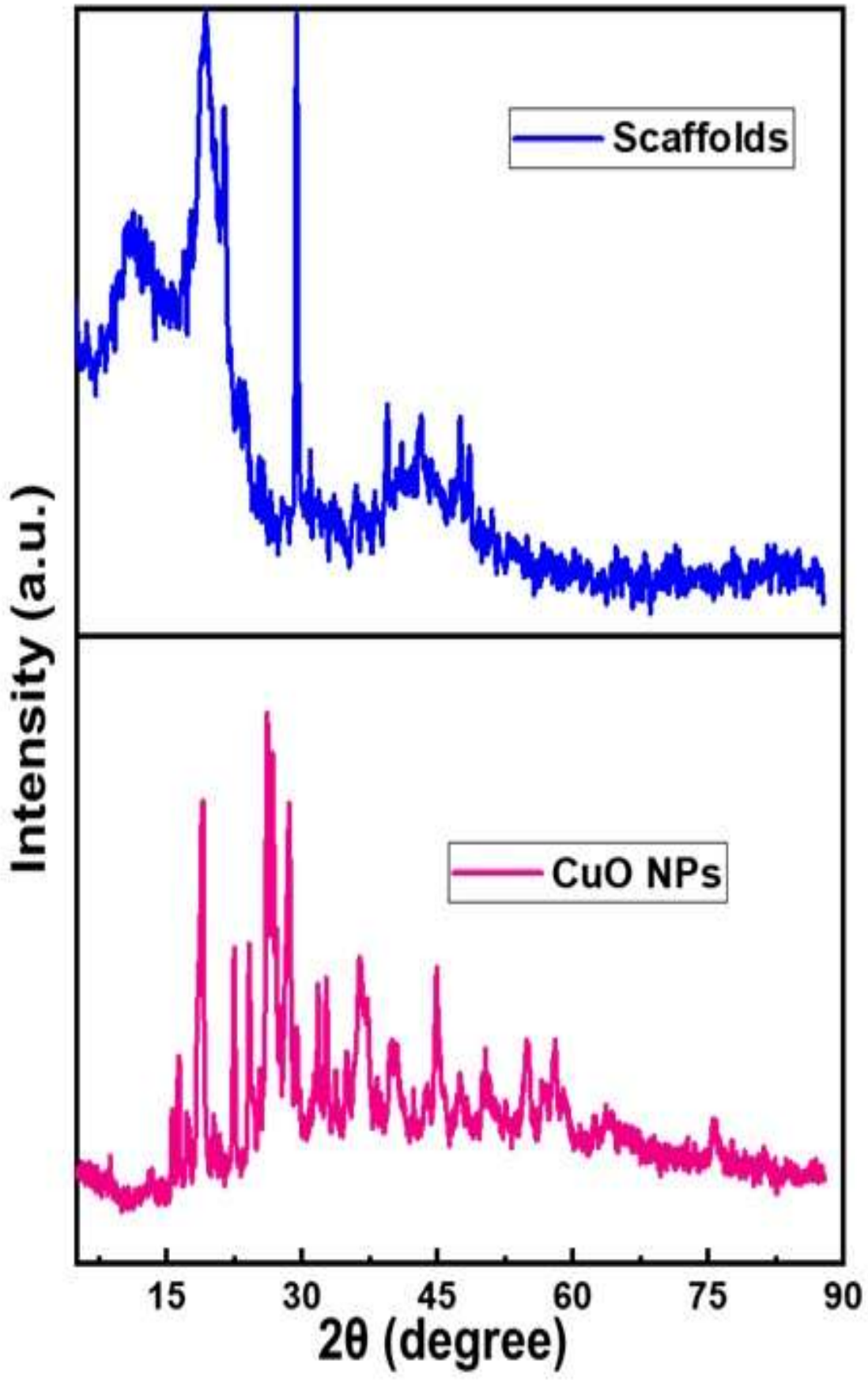

Fig. 3. XRD patterns of synthesized CuO NPs and CuO-loaded scaffolds.

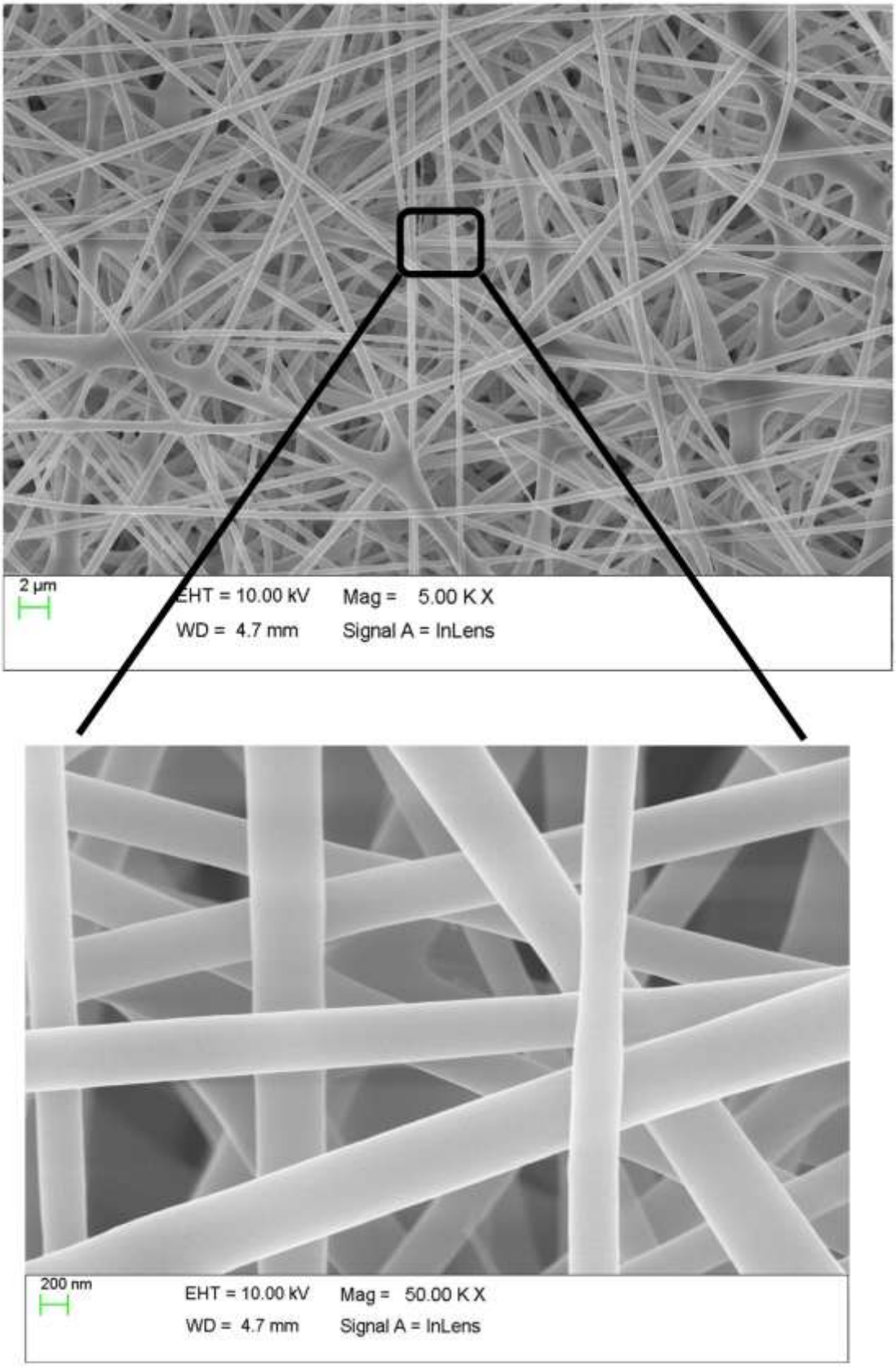

Fig.4. SEM analysis of starch/PVA/CuO-NPs nanoscaffolds

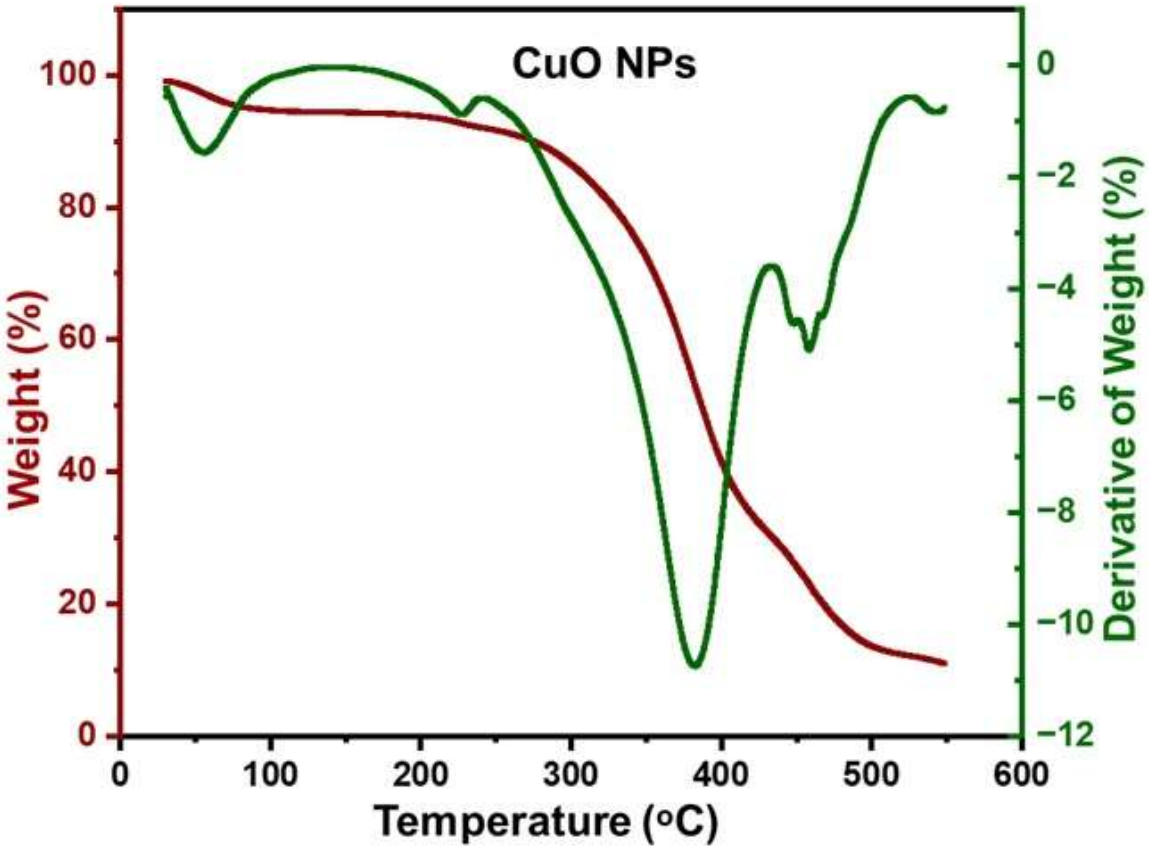

Fig. 5. Thermal degradation behavior of CuO-incorporated nanoscaffolds.

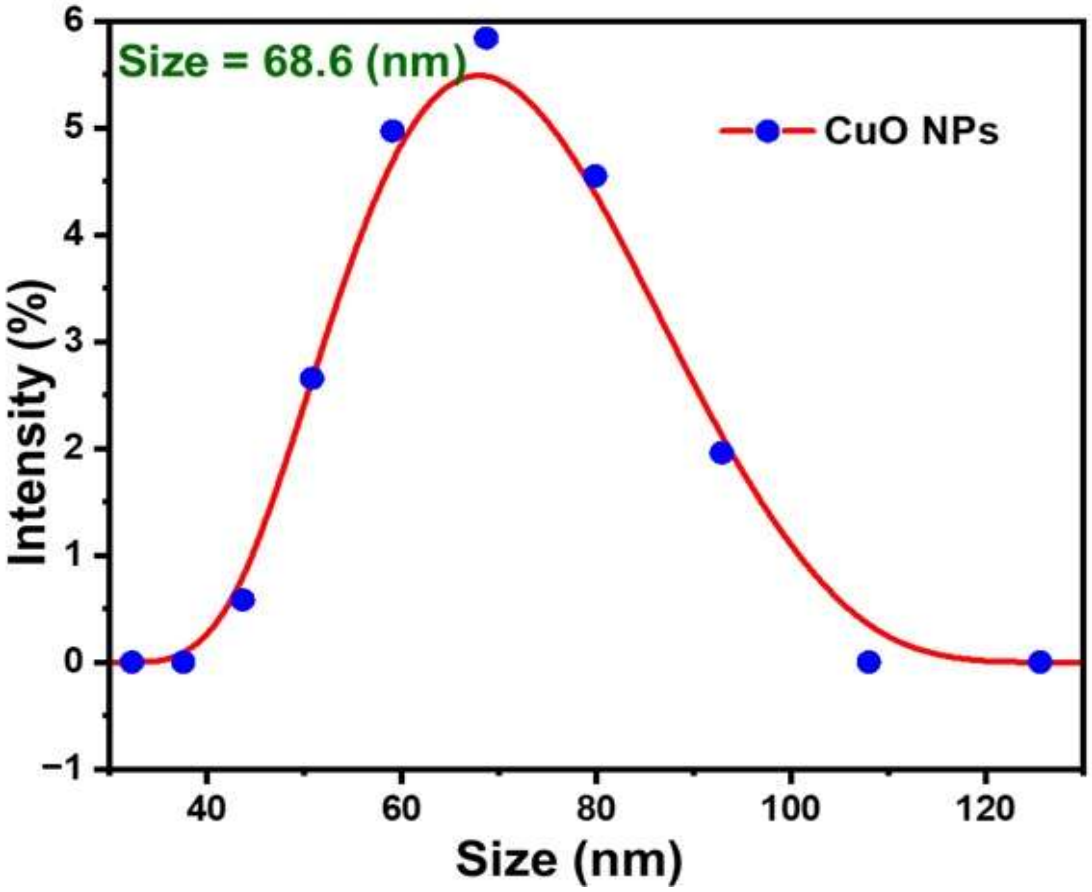

Fig.6. DLS particles size analysis of CuO NPs

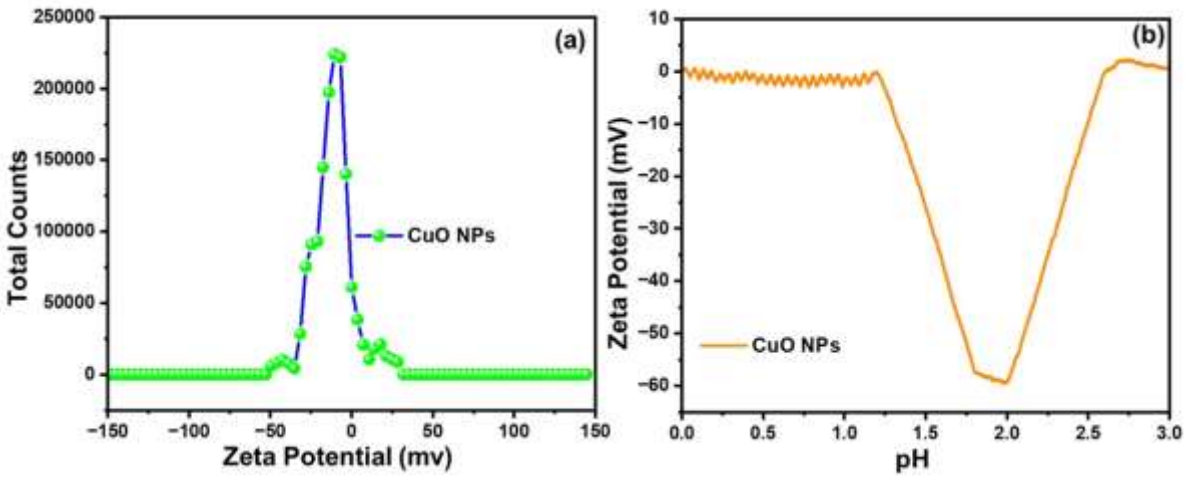

Fig.7. Zeta-potential analysis of CuO NPs

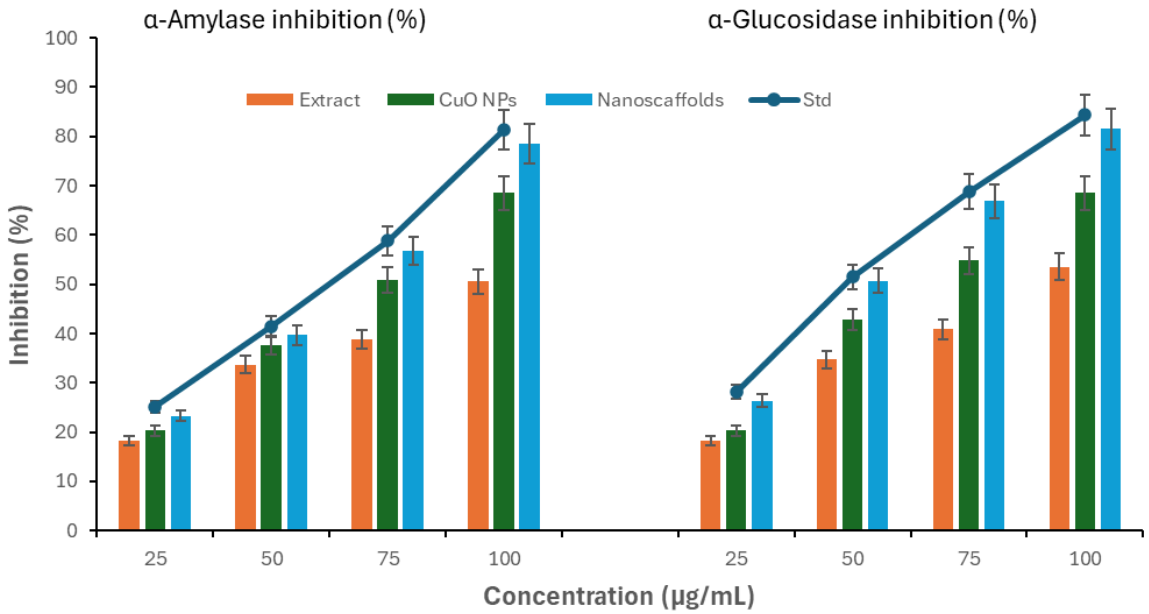

Fig.8. Antidiabetic activity analysis of algal extract, CuNPs and starch/PVA/CuONPs nanoscaffolds